Research Square

Preprints are preliminary reports that have not undergone peer review.
They should not be considered conclusive, used to inform clinical practice,
or referenced by the media as validated information.

The predictability barrier of climate instabilities

Anders Levermann

anders.levermann@pik-potsdam.de

Potsdam Institute for Climate Impact Research https://orcid.org/0000-0003-4432-4704

Nina Doerfler

Potsdam Institute for Climate Impact Research

Article

Keywords:

Posted Date: November 9th, 2026

DOI: https://doi.org/10.21203/rs.3.rs-11278028/v1

License: This work is licensed under a Creative Commons Attribution 4.0 International License.
Read Full License

Additional Declarations: There is **NO** Competing Interest.

The predictability barrier of climate instabilities

Nina Doerfler[1,2,3*] and Anders Levermann[1,2,3*]

[1*]Department of Complexity Science, Potsdam Institute for Climate Impact Research, Telegrafenberg A56, Potsdam, 14473, Germany.
[2]Institute of Astronomy and Physics, Potsdam University, Karl-Liebknecht Strasse 24-25, Potsdam, 14476, Germany.
[3]Department of Integrative Earth System Science, Max Planck Institute of Geoanthropology, Kahlaische Str. 10, Jena, 07745, Germany.

*Corresponding author(s). E-mail(s): nina.doerfler@pik-potsdam.de; anders.levermann@pik-potsdam.de;

Abstract

Anthropogenic warming bears the risk of climate instabilities, some of which might have already been initiated. Due to their multidecadal to millennial transition times, their interaction with weather has rarely been investigated and their discounted economic impact has been considered relatively low. Here we show that (1) even rapidly changing, i.e. weather-induced, forcing influences systems with multidecadal collapse times such as the Atlantic overturning and the Amazon rainforest, (2) approaching their tipping temperature immediately increases weather-induced volatility long before the tipping point is reached and well after the tipping point is passed, (3) unpredictability of these systems is further increased by noise-enhanced tipping and (4) for multidecadal systems variability increases by up to 120% and unpredictability by more than 300%. The faster the internal system time the stronger the increase in variability and unpredictability. Thus, in addition to the fundamental long-term changes, volatility poses an immediate societal and economic risk from climatic tipping that is directly related to the tipping process itself.

Keywords: Global warming, Instabilities, Economic risk, Weather variability

1 Introduction

Self-amplifying feedbacks within climatic subsystems such as the Atlantic meridional overturning circulation or the ice sheets on Greenland and Antarctica may lead to threshold behaviour in the response of these systems to global warming [1, 2]. Some of the corresponding tipping temperatures might have already been passed [3–6]. Research has so far focused on investigating the mechanism of the instability [7–10], detecting the tipping points [11–14], developing early warning [11, 15, 16], understanding the fundamental change that is associated with the qualitatively different state that emerges [17–19] and the cascading effects between different tipping elements [20–22]. Due to the decadal- to millennial-scale transition times of the tipping elements, macro-economic consequences have often been estimated to be small due to discounting [23–25]. Recently, we suggested that variability of these systems close to the tipping point might make societal and economic relevance of these instabilities immediate [26].

In situations where the system dynamics is faster than the increase in global temperature, i.e. the gradual forcing, this variability is well-known from the detection of early warning signals (EWS) based on critical slowing down (CSD). As a system approaches an instability its restoring ability weakens, which leads to stronger and longer lasting deviations from its mean state. While CSD has been used to detect EWS [1, 12, 15, 27, 28], systems with a long internal time scale compared to the forcing time scale are not expected to exhibit EWS [29], [30], [31]. The growth of fluctuations that informs us about the approach of a tipping point come with their own cost: the loss of short-term predictability [26]. The more a system fluctuates, the harder it becomes to predict its state a few years ahead. With several tipping elements already showing signs of destabilisation, it is not only relevant whether tipping approaches, but also how unpredictable a tipping system will become and how this influences the climate system around it, both before and beyond the tipping point.

Here, we differentiate between two sources of unpredictability. Fluctuation-driven unpredictability is caused by the variability around the mean state captured by CSD. Trajectory-driven unpredictability arises once the system is destabilised. Small weather-induced perturbations are then no longer damped but can siginificantly alter the future evolution of the system, because in the vicinity of the instability the system dynamics response strongly asymmetrically to forcing, i.e. the weather-induced noise. We use a generic saddle-node-bifurcation equation to analyse its unpredictability along the whole tipping process and most importantly for interacting time scales, i.e where a 'separation of times scales' is not possible (for a list of systems that obey such a bifurcation see Supplementary Note 1). We find a predictability barrier, lying between the tipping point and the point of no return. For systems with transition times of about 50 years such as the Atlantic Overturning Circulation (AMOC), the fluctuation variance increases by up to 150% and the uncertainty in the 10 year state evolution by more than 300%. We derive an analytic expression for the predictive uncertainty in such systems and show that fluctuation-driven unpredictability dominates until shortly after the tipping point and trajectory-driven unpredictability afterwards. The risk of tipping elements for society thus does not only lie in the transition to a different state but also in the unpredictability caused by the destabilisation of the tipping element throughout the tipping process.

2 Weather-induced fluctuations

Although details of the instabilities associated with different tipping systems might be different, the generic representation of tipping dynamics can be captured by a saddle node bifurcation. We use its normal form with red noise as detailed in the Methods. A list of systems that follow this normal form is provided in Supplementary Note 1. The system state is denoted by x and the forcing which represents the temperature increase by θ. We will use the relative forcing with respect to the critical forcing, $T = \theta/\theta_c$. In order to investigate their interaction we specifically represent and distinguish four time scales. The correlation time scale of the noise is associated with weather variability. It is the fastest time scale and is fixed to $\tau_n = 10\,\text{days}$. Throughout the paper we use a forcing time scale of $\tau_f = 125\,\text{yr}$, defined as the time it takes to reach the tipping temperature $\theta = \theta_c$ or $T = 1$. In order to investigate the societal relevance we set a prediction horizon of $\tau_p = 10\,\text{yr}$ which however is mostly relevant for analysis purposes. The central time scale for this study is the that of internal system dynamics τ_s. It is the parameter linearly related to the internal response time.

With increasing forcing T, the system undergoes a tipping transition with or without weather-induced noise (Fig. 1a, gray and black lines). If weather is present it provokes a variability in the system (Fig. 1a, red line and uncertainty range) which increases when approaching the tipping temperature because the time-dependent internal relaxation time $\tau(t) = \tau_s/\partial_x f(x(t), \theta)$ becomes larger (see Methods). This mechanism is generally considered critical slowing down (CSD). In early warning of tipping it is assumed that the system time scale is slow compared to weather, but fast enough to respond to its variability. Along its trajectory the system undergoes three qualitatively distinct points: the tipping temperature, the tipping point and the point of no return.

The **tipping temperature** (or tipping forcing) is the forcing value at which the system destabilises if this forcing were to be maintained at this level. It is a value of the control parameter θ. In the governing equation this is the forcing at which the current equilibrium ceases to exist (Fig. 1 b).

The **tipping point**, in distinction, is a value of the state variable x which is reached if the temperature is maintained at or above the tipping temperature for long enough for the system to indeed become unstable. Most climatic subsystems have inertia and thereby the tipping point is reach significantly later than the tipping temperature. As soon as the system crosses the tipping point, the self-amplifying feedback [32] pulls it to the new attractor. Beyond the tipping point, the system stops lingering in the vicinity of the 'ghost' of the old equilibrium and starts accelerating towards the new equilibrium (Fig. 1 b). The transition time between the tipping temperature and the tipping point depends on the internal time scale of the system τ_s and the forcing time scale τ_f and will be further discussed in Fig. 3.

The **point of no return** (POR) [33] is the system state after which the tipping process can not be reversed anymore, even if the forcing was immediately set back to the initial value. In the climate system this translates to the system state beyond which the system would collapse even if global mean temperature would go back to

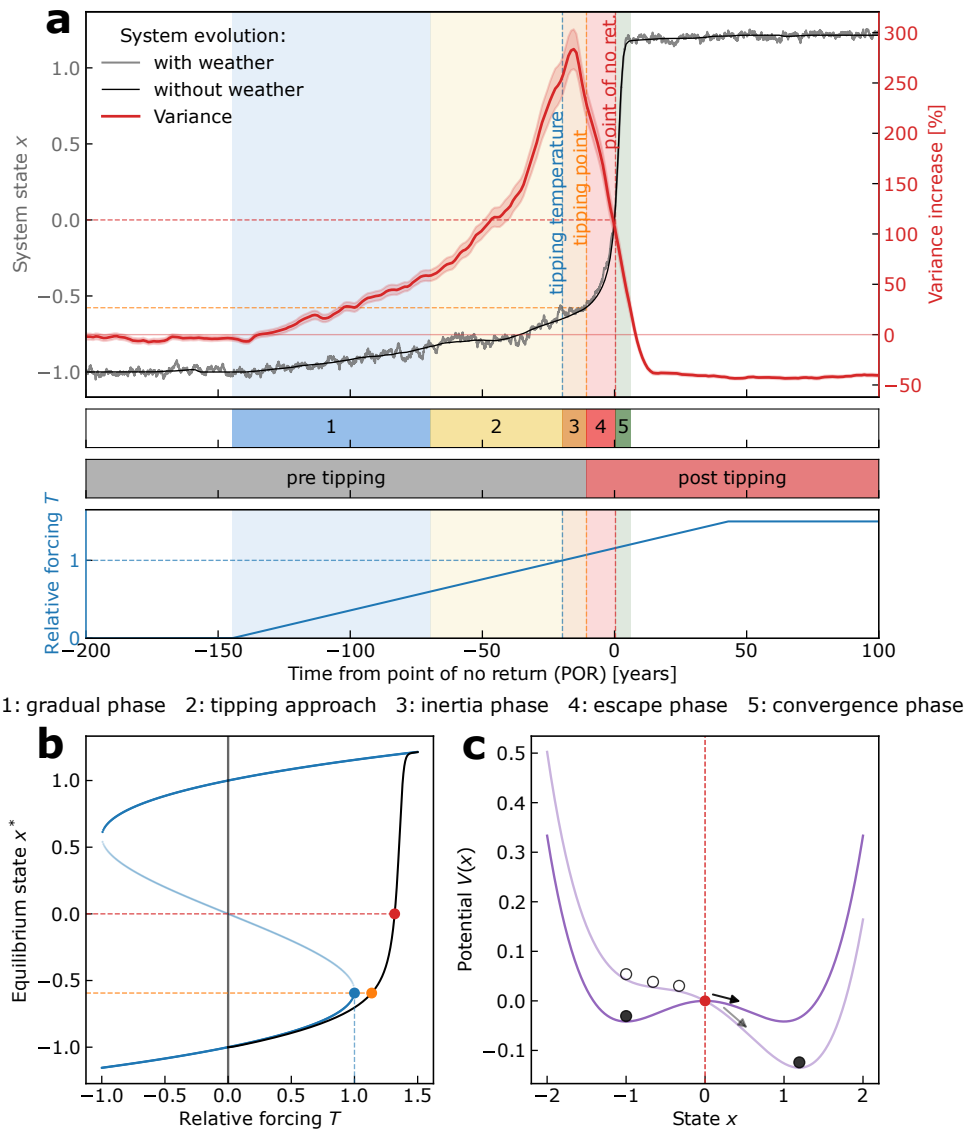


Fig. 1 Temporal evolution of weather induced variance while a system undergoes tipping. The internal time scale of the system is $\tau_s = 1\,\mathrm{yr}$, the forcing time $\tau_f = 125\,\mathrm{yr}$, the noise time $\tau_n = 10\,\mathrm{days}$. a) Exemplary trajectory with weather (gray) and the locally fitted deterministic trajectory without weather (black) used for detrending (Methods), plotted over time relative to point of no return ($x = 0$). The relative forcing T is shown in blue in the lower panel, the tipping temperature is crossed at $T = 1$. The mean increase in variance of the system with weather relative to its initial value is shown in red with its standard error. Variance increase peaks at 300% after the tipping temperature is crossed. Tipping temperature (blue), tipping point (orange) and point of no return (red) are marked by dashed lines, horizontal dashed lines give the corresponding system state. Tipping phases (Methods) are represented by shading in the back and named underneath the panel. b) Bifurcation diagram, with equilibrium state x^* plotted over relative forcing T. At the crossing of the tipping temperature (blue), the old equilibrium ceases to exist, but the trajectory (black) lingers close to it throughout the inertia phase, until it reaches the tipping point (orange). Point of no return marked in red. c) Potential landscape. Solid purple line is at zero relative forcing $T = 0$. Increasing forcing changes the potential (light purple line) and the equilibrium state (black dots) until the old equilibrium vanishes. Once the point of no return (red) has been reached, the system falls into the other equilibrium, even if T is suddenly set back to zero.

pre-industrial values (red dot in the potential landscape of Fig. 1 c corresponding to $x_{POR} = 0$).

Already for the fast system with $\tau_s = 1\,\mathrm{yr}$ depicted in Fig. 1, the maximum variance increase of 300% occurs significantly *after* the tipping temperature, in the inertia phase between the tipping temperature and the tipping point. Thus short-term unpredictability, as represented by the variance, peaks in the inertia phase, in which the system is still lingering close to its old equilibrium, but has lost its attraction point to relax to after a perturbation. In this sense, the system is already in a state of free fall [26], in which perturbations can not be damped anymore and the system is highly unstable. For slower systems the variance peaks at higher and higher system states (Fig. 2). Unpredictability starts to decrease again in the attraction phase, after the POR where the fluctuations get damped by the strong drift towards the new equilibrium, but even at the POR the variance is still 100% above its initial value for $\tau_s = 1\,\mathrm{yr}$. Once the system settles in its new equilibrium, the fluctuation variance also settles to its new equilibrium value.

An analytic approximation of the dynamics around the tipping point [30, 34, 35] yield a universal scaling of the transition time between the tipping temperature (TT) and the POR with the system- and forcing time scales

$$t_{trans} \equiv \Delta t = t_{por} - t_c \sim \tau_f^{1/3} \tau_s^{2/3}. \tag{1}$$

This theoretical prediction (lines in Fig. 3) captures the median in an ensemble of 100 simulations very well (solid circles in Fig. 3) as well as the deterministic values (open circles). For further information on the derivation of the scaling law we refer to the Methods and the Supplementary Note 2. For the inertia phase, the scaling law reproduces the delays for the system without weather induced noise across the full range of system time scales τ_s (Fig. 3 b). Noise shortens this phase, since it can induce early transitions, reducing the stochastic median of the delays compared to a system without noise. The spread of the delays is higher for systems with larger internal time scales. Since slow systems have weak restoring capabilities, different noise realisations lead to a larger spread in possible trajectories and delay times. In the escape phase, from the crossing of the tipping point to the point of no return, the scaling still captures the delay in a noise free system for small τ_s (Fig. 3 c). It becomes less accurate for higher τ_s, where the point of no return is only reached after the ramp up of the forcing and we are thus in a dynamically different regime. However here the median of the delay of the noisy trajectories is higher than that of the system without weather variability. The two deviations largely cancel each other in the total transition time, i.e. the time the system takes to reach the point of no return after crossing the tipping temperature (Fig. 3 a). The median total transition time, spanning the inertia and the escape phases, thus behaves as a robust property of the system.

Since the transition time depends on the internal time scale of the system, a system with higher inertia takes significantly longer to complete its transition to the point of no return and then to the new equilibrium state. For slowly responding

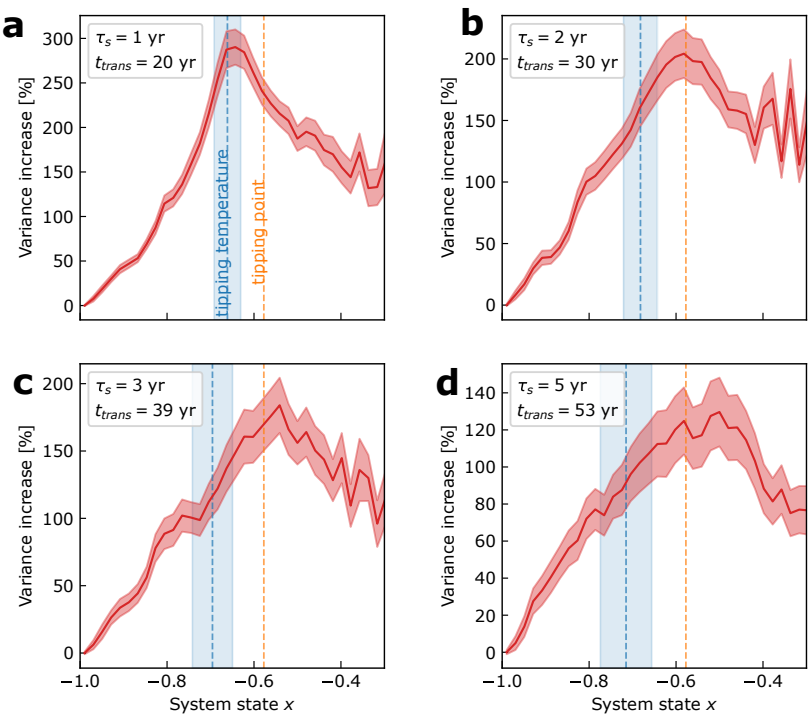


Fig. 2 Variance as a function of system state. Increase in variance of the ensemble (Methods), computed in bins of system state x and shown relative to the initial variance. The red lines show the mean, the shading its standard error. The crossing of the tipping temperature (dashed blue line) occurs at different system states depending on the realisation. Its standard deviation is shaded in blue. The tipping point is shown as orange dashed line. Noise and forcing time scales are chosen as in Fig. 1, the system time scale is a) $\tau_s = 1\,\mathrm{yr}$, b) $\tau_s = 2\,\mathrm{yr}$, c) $\tau_s = 3\,\mathrm{yr}$ and d) $\tau_s = 5\,\mathrm{yr}$. The transition time is the median time the system takes to reach the point of no return after the tipping temperature is crossed (see Fig. 3). In all cases, the maximal variance is reached after the tipping temperature is crossed. Slower systems have a lower maximal variance, which is reached at later system states.

climate tipping points like ice sheets, the transition time could be several hundred to thousands of years. The scaling also shows us that the time climate tipping points take to complete the transition, depends on the rate of the forcing $1/\tau_f$. Comparing the scaling exponents to each other, however, the forcing rate has a considerably smaller influence than the inertia of the system. This reflects the dominance of the self-amplifying feedback that generates the tipping [32].

For a system to exhibit CSD, its internal relaxation time needs to be short compared to the forcing timescale. When this separation breaks down, the system lags behind the instantaneous equilibrium and fluctuations can no longer reflect the local restoring rate at that equilibrium. The important property here is the *ratio* between the forcing timescale and the system timescale. This also has implications for the importance of the rate of warming: the faster the warming, the less climate components can track their equilibrium state, and the weaker the CSD signals we can expect.

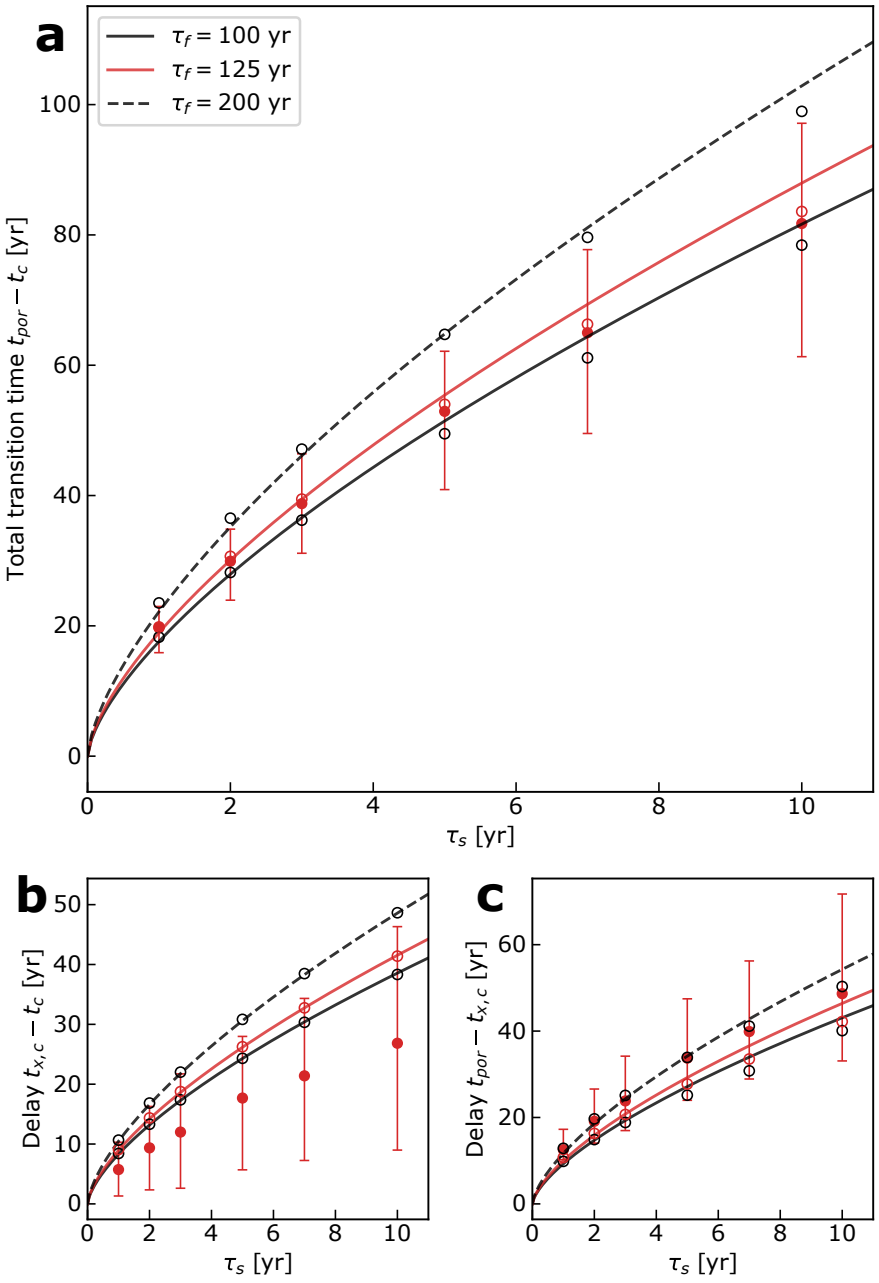


Fig. 3 Scaling of the transition time with system time scale τ_s and forcing time τ_f. System time values are $\tau_s \in \{1, 2, 3, 5, 10\}$ years and forcing times $\tau_f \in \{100, 125, 200\}$ years. Lines represent the theoretical scaling Eq. (1), hollow dots are the delays read off the trajectories without noise. For $\tau_f = 125\,\mathrm{yr}$, solid dots show the median of the delays over the ensemble of $n = 100$ stochastic realisations, with the error bars spanning the likely range (66%). The times at which the tipping temperature, tipping point and point of no return are reached are denoted t_c, $t_{x,c}$, t_{por}. a) Total transition time from crossing the tipping temperature to the point of no return. b) Delay between the tipping temperature and tipping point (inertia phase). c) Delay between the tipping point and point of no return (escape phase). Weather variability shortens the inertia phase, but lengthens the escape phase, making the total transition time relatively insensitive to noise.

However, weaker CSD signals do not imply a predictable transition. Instead, a new measure is needed; one that does not rely on a separation of time scales, but instead captures all weather induced contributions to the unpredictability of a system. This measure is especially important for the assessment of unpredictability of the system after it has crossed its tipping point.

3 The predictability barrier

To capture the full unpredictability of the system, we use the spread of all trajectory evolution starting from a given state of the system over a given prediction time horizon. We choose 10 years as this time horizon, i.e. we ask the question: based on the current system state, what is the spread of possible systems states in 10 years? The specific horizon was chosen to be relevant for society, both for mitigation and adaptation strategies, but it has an arbitrary component to it and may be chosen differently.

The spread of possible future states encompasses both the systematic drift of the system towards the new state and the spread of possible trajectory evolutions caused by weather variability (Fig. 4 a). Removing the 10 year change the system would experience without weather variability isolates the latter (Fig. 4 b). Depending on the current state of the system, the spread in possible evolutions in the future 10 year window differs substantially (Fig. 4 c-e). Far from the tipping temperature, trajectories mainly differ from each other by fluctuations around the mean state, which increase towards the tipping temperature (Sec. 2). After the tipping point is reached, the spread becomes much larger (Fig. 4 d). For a system time scale of $\tau_s = 1\,\mathrm{yr}$, the prediction within 10 years after the tipping point varies between the system being fully tipped and not tipped at all, depending on the exact realisation of the weather variability. The unpredictability at a given state x_t is further quantified as the likely range of trajectory spread (orange lines in Fig. 4 a,b) in Fig. 5.

For all system time scales, we find a barrier of unpredictability after the tipping point and before the POR, in which the 10 year prediction of the system becomes most uncertain. We derive a theoretical estimate of this unpredictability barrier through the trajectory variance, locally linearised around the deterministic solution as described in the Supplementary Note 3. Its temporal evolution follows

$$\frac{dV}{dt} = -2\frac{V(t)}{\tau(t)} + 2\sigma^2\tau_n\frac{\tau(t)}{\tau(t)+\tau_n} \approx -2\frac{V(t)}{\tau(t)} + 2\sigma^2\tau_n. \tag{2}$$

where $\tau(t) = -1/\lambda(t)$ is the time dependent relaxation time of the system with $\lambda(t) = \partial_x f(x,\theta) = (1-3x^2)/(2\tau_s)$ being the local growth rate of perturbations. The last approximation holds whenever the noise is much faster than the system, i.e. time scale of the system $\tau(t)$ is much larger than the time scale of the noise $\tau(t) \gg \tau_n; \forall t$. We thus extend the fluctuation variance from Sec. 2 (Fig. 1, Fig. 2) by intentionally not aligning trajectories, but instead including their spread as their major cause for unpredictability.

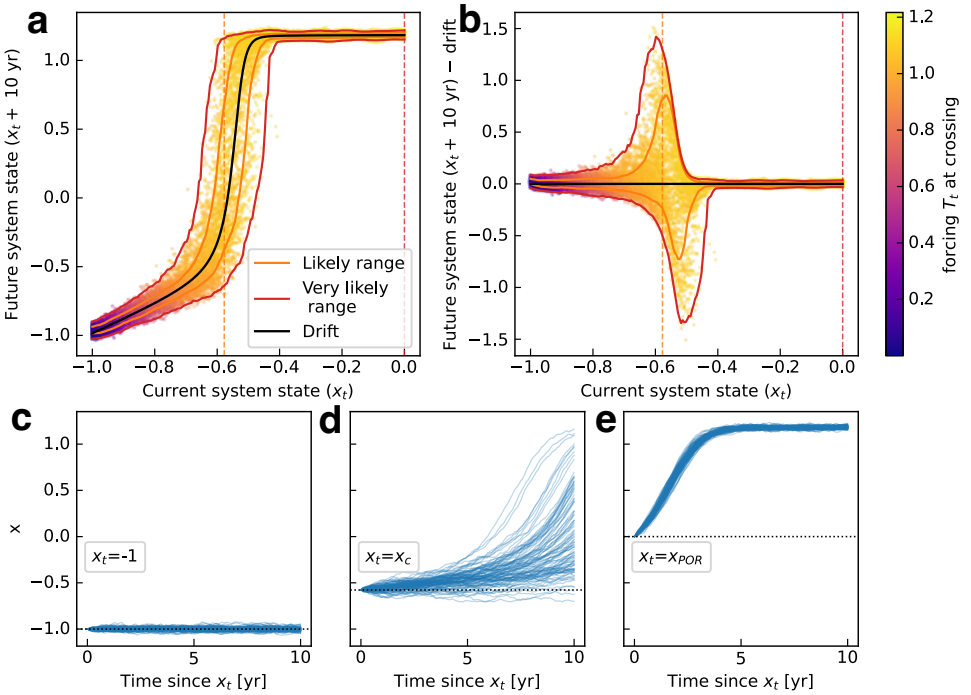


Fig. 4 Predictability of the future system state. All panels are for system time scale $\tau_s = 1\,\mathrm{yr}$. a) Possible system states 10 years ahead $x_t + 10\,\mathrm{yr}$ as a function the current system state x_t. Point color gives the relative forcing T at current time t. Solid orange lines span the likely range (66%) and solid red lines the very likely range (90%). The black line shows the mean drift of the system without weather. b) As a), with the mean drift subtracted, giving only the weather induced unpredictability. The orange dashed line shows the tipping point, the red dashed line the point of no return. c)-e) Possible future trajectories over the next 10 years, starting from c) the initial state $x_t = -1$, d) the tipping point $x_t = x_c$ and e) the point of no return $x_t = x_{POR}$. The spread of possible trajectories rises sharply after the tipping point and is small far from it and beyond the point of no return, since for this fast system a large part of the transition falls within the 10 year prediction window.

The first term in the variance equation describes how fluctuations grow or decay locally, depending on the sign of the restoring force $\partial_x f(x, \theta)$. The second term is a constant noise contribution. In the framework of critical slowing down, the weakening of the restoring force is usually used to indicate the approach of the tipping temperature. In that sense, before the tipping point, the variance equation still partly describes the fluctuation variance, since trajectories do not yet deviate strongly from each other. After the tipping point, the variance is instead dominated by deviating trajectories, so unpredictability mainly stems from the large spread of possible trajectories.

Integrating the variance equation forward by 10 years for current state x_t, yields the theoretical curves in Fig. 5. They reproduce the position of the maximum and shape of the predictability barrier. In fact, the existence and location of the predictability barrier follows directly from the variance equation. The damping of

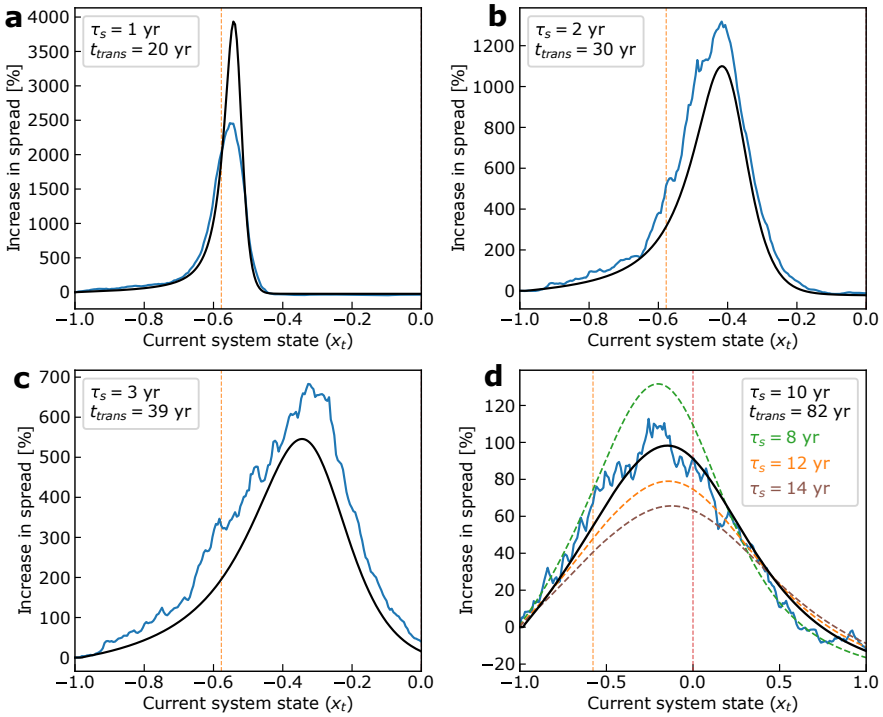


Fig. 5 Loss of predictability during tipping. Increase in the 10 year spread relative to its initial value, plotted over the current state x_t. Blue shows the width of the likely range (66%, cf. green lines in Fig/ 4). Black lines show theoretical predictions, obtained by integrating Eq. 2 forward by 10 years from each x_t. The orange dashed line shows the tipping point, the red dashed line the point of no return. The system time scales are a) $\tau_s = 1\,\text{yr}$, b) $\tau_s = 2\,\text{yr}$, c) $\tau_s = 3\,\text{yr}$ and d) $\tau_s = 10\,\text{yr}$ together with additional theoretical curves for $\tau_s = 8\,\text{yr}$ (green), $\tau_s = 12\,\text{yr}$ (orange) and $\tau_s = 14\,\text{yr}$ (brown). The legend shows system time scales and transition times (Fig. 3). For slower systems, the peak loss of predictability gets lower and moves from shortly after the tipping point to the point of no return.

perturbations weakens as the system approaches the critical point x_c, vanishing entirely once it is reached. Beyond the critical point, the restoring force actually becomes positive: small perturbations are no longer damped but actively amplified and the restoring force becomes an amplification force. Due to the strong asymmetry of the system dynamics in the escape and convergence phases (Fig. 1 and Methods) a small perturbation can therefore significantly deviate the trajectory, making the system's future state much harder to predict.

Comparing the different system time scales, fast systems show a very sharp and high predictability barrier just after the tipping point, while for slower systems the maximum decreases and shifts towards the POR. This difference depends on a new relevant ratio of time scales: the length of the forecast window time relative to the system's internal time scale. How pronounced the barrier of unpredictability is then depends on how much of the transit through the unstable regime falls within the 10 year window. For systems that transit through the destabilised regime quickly

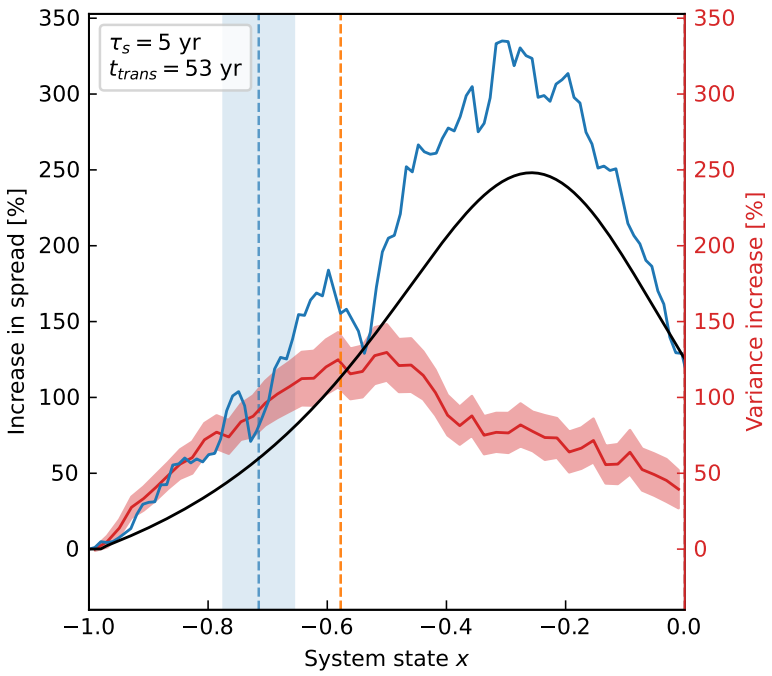


Fig. 6 Unpredictability decomposition for $\tau_s = 5\,\text{yr}$. In one of the most relevant cases that is associated with a transition time in the vicinity of $t_{trans} = 50\,\text{yr}$ the increase in 10 year spread (blue, theoretical estimate in black, cf. Fig. 4) closely follows the increase in fluctuation variance (red, cf. Fig. 2) up to slightly after the tipping point. Beyond that, the fluctuation variance declines, while the spread increases to more than twice the fluctuation variance increase. Early in the transition, the loss in predictability thus mainly reflects the increased variability. The tipping temperature is shown by the dashed blue line (with standard deviation shaded) and the tipping point by the orange dashed line.

compared to the window length, the largest spread occurs shortly after the tipping point, since the window can then capture most of the escape and convergence phase, and thus the full spread of trajectories (Fig. 4 d). For systems with slow internal time scales, the trajectory barely changes within 10 years, so the local growth rate $\lambda(x_t)$ stays roughly constant. In this case, the spread measured over the 10 year horizon simply reflects how much this constant local growth rate force amplifies the spread in trajectories over the fixed window. Since this amplification is strongest at the POR ($x_t = 0$), the maximum variance shifts towards that system state as the internal time scale increases. The predictability barrier for fast systems is thus governed by how much of the destabilised regime the 10 year window can capture, while for slow systems it is governed by how locally unstable the system is at the moment the forecast begins.

Systems with intermediate time scales combine both types of unpredictability (Fig. 6). These are system time scales that are highly relevant for climate tipping

points. For $\tau_s = 5\,\mathrm{yr}$, the transition time is about 50 yr, comparable to the time scale estimated for the AMOC shutdown [2]. For such a system, the increase in the 10 year spread closely follows the increase in fluctuation variance until slightly after the tipping point (Fig. 6). Beyond that, the fluctuation variance declines, while the trajectory spread increases to more than twice the variance increase. The same weather variability thus leads to different types of unpredictability depending how far the tipping process has advanced. Until shortly after the tipping point, increasing fluctuations around the mean state make the system more unpredictable. After that, the phase of largest unpredictability begins. Weather variability can now push the system onto a wide span of trajectories, making the 10 year prediction highly uncertain.

4 Discussion

We consider climatic tipping processes in a time scale regime relevant for society, i.e. with forcing time scales of the order of 100 years and prediction time scales relevant for society of the order of 10 years. Within this framework, we find that for relevant systems such as the Atlantic overturning circulation and the Amazon rainforest, the theoretically simpler separation of time scales between system dynamics and forcing rate becomes more difficult. Instead the time scales strongly interact which makes it necessary to introduce a new measure for unpredictability. Two mechanisms contribute to this unpredictability. Up to and slightly beyond the tipping point, growing fluctuations around the mean state make the future state less predictable. Beyond that, unpreditability is dominated by the large spread of possible weather-induced trajectories through the regime in which the system is destabilised. We use a 10-year horizon as a reasonable planning horizon for human societies.

Existing work has asked the questions of whether [2, 15, 36, 37] and when [38] a state will tip and how predictable the final state will be [39]. The unpredictability of the transient state has received little attention. For planning, it is highly relevant to have an estimate of how unpredictable a given climate component will be, based on its current state. The framework presented here quantifies this state dependent unpredictability through every phase of the transition.

The inertia associated with the internal time scale of the system determines how this unpredictability unfolds. The importance of time scales has been discussed for temporary threshold crossing of slow-onset systems [40, 41]. Climate tipping points are usually identified by their tipping temperature, which obscures the fact that their transition times vary vastly [40]. The distinction between tipping temperature, tipping point and point of no return introduced here makes the role of inertia explicit. Elsewhere, the point of no return is defined dynamically, with a dependence on the forcing pathway [33]. The definition used here generalises this concept to allow the definition of tipping phases that is independent of the exact forcing scenario, defining the latest possible point of no return.

The internal time scale also shapes the barrier of unpredictability. Fast systems show a sharp, high barrier just after the tipping point, while for slower systems the barrier is lower and shifts towards the point of no return. Before the tipping point, the internal time scale determines whether the system exhibits pronounced CSD, which requires the system to relax faster than the forcing changes [29–31]. For very slow systems, detecting a signal would require observational records that are much longer than those available [42]. The predictive capacity for real world climate components is further limited by observational uncertainties [43]. Where CSD occurs, it only captures the first part of the loss of predictability. Especially in the wake of the discussion about the importance of rate-dependent tipping [44–46], CSD might not be the defining signature of tipping points anymore [47]. Instead, the weather induced spread in trajectories becomes even larger, with some trajectories tipping and others not. In more complex models, ensemble splitting, where only part of the trajectories tip, as well as chaotic dynamics and multiple states have been observed [47–49]. The results presented here are therefore likely a lower bound of unpredictability.

The generic saddle-node model used here is not meant to reproduce the exact behaviour of specific tipping elements. Instead we aim to discuss unpredictability in a generic sense that is conceptually relevant for a large number of systems. The dynamics here are simplified and weather is represented as additive noise of fixed intensity and correlation time. We assume a linear ramp up of forcing and do not include a ramp down, i.e. an overshoot scenario. The existence of rate-induced and noise-induced tipping is not explicitly analysed. Further work is required to expand the framework to specific climate components. In a world where the tipping temperatures of several tipping elements are crossed, these components can be expected to become much less predictable. This will play out leading up to but also especially after the crossing of the tipping point where the system is in a free fall state and small weather-induced perturbations have a large influence on its future trajectory.

5 Methods

Running variance

The fluctuations around the mean state along the whole trajectory is analysed by detrending the stochastic trajectories by subtracting a locally time-shifted deterministic reference trajectory x_{det}. The time shift is chosen to minimises the square error of the mean (MSE) residual between the time shifted pieces of the deterministic trajectory and the stochastic trajectory within a sliding window. Due to the non-linear temporal evolution in the vicinity of the tipping point, this detrending was preferred over linear-detrending. Both methods give very similar results.

$$shift = \mathrm{argmin}_s \frac{1}{N} \sum (x_{stoch}[i : i + W] - x_{det}[i + s : i + W + s])^2. \quad (3)$$

Here x_{stoch} is the stochastic trajectory, N the number of members in the ensemble, W the window size. To get the mean variance of the ensemble in Fig. 1, the trajectories are aligned along the point of no return. Then the average of the variance across all trajectories is taken.

Binned variance

Instead of aligning trajectories to each other in time as in Fig. 1 a, in Fig. 2 we bin the mean fluctuation variance of the ensemble over the current mean state $x_{det,\text{shifted}}$ (one for each stochastic simulation, determined by the procedure above). This places all simulations and all values of τ_s on a common axis.

The variance of each detrended stochastic simulation (see above) is determined and plotted over its locally fitted deterministic trajectory that was used for detrending $x_{det,\text{shifted}}$. Since different simulations are sampled at different values of x, we estimate the mean variance on a grid of bins of equal width. To make sure that each simulation contributes equally within each bin, first the mean of the values of each simulation in one bin b is taken

$$\bar{V}_{i,b} = \frac{1}{n_{i,b}} \sum_k V_{i,k} \tag{4}$$

where $n_{i,b}$ is the number of values of simulation i in bin b. We then average across simulations within each bin

$$\bar{V}_b = \frac{1}{N_b} \sum_i \bar{V}_{i,b} \tag{5}$$

where N_b is the number of simulations that are present in a bin. The standard error of the mean binned variance $\bar{V}_b$ is then given by the sample standard deviation across simulations $\text{SEM}_b = \text{STD}(\bar{V}_{i,b})/\sqrt{N_b}$. The increase of variance is taken relative to the first bin $(\bar{V}_b/\bar{V}_{b_0} - 1) \cdot 100$.

Saddle node bifurcations

Throughout the paper we use a generic cusp normal form, in which tipping occurs through a saddle node bifurcation.

$$\frac{dx}{dt} = \frac{x_0}{2\tau_s}\left(-\left(\frac{x}{x_0}\right)^3 + \frac{x}{x_0} + \theta(t)\right) + \xi(t) \equiv f(x, \theta, \xi) \tag{6}$$

$$\frac{d\xi}{dt} = -\frac{1}{\tau_n}\xi + \sqrt{\frac{2\sigma^2}{\tau_n}}\eta(t) \tag{7}$$

with x describing the system state, θ the external forcing and $\xi(t)$ the red noise. x_0 is a scale that can be set arbitrarily and is set to $x_0 = 1$ and does not enter any relevant

result but is physically necessary to carry in a dimensional analysis (Supplementary Note 1). The second equation describes the dynamics of the red noise with time scale τ_n, and stationary variance σ, where $\eta(t)$ stands for temporally uncorrelated, white noise. The internal time scale parameter, τ_s, is the time scale at which perturbations relax at zero forcing $b = 0$. As soon as the system is forced, the internal relaxation time becomes time-dependent

$$\tau(t) = -\frac{\partial}{\partial x} f(x, \theta, \xi) = \frac{3(x/x_0)^2 - 1}{2\tau_s}. \tag{8}$$

The deterministic ODE can also be described as the negative derivative of the double well potential (cf. Fig. 1 c)

$$U(x) = \frac{x_0}{2\tau_s}\left(\frac{1}{4}\left(\frac{x}{x_0}\right)^4 - \frac{1}{2}\left(\frac{x}{x_0}\right)^2 - \theta t\right). \tag{9}$$

Setting $f(x) = 0$ and $\partial_x f(x, \theta, \xi) = 0$ yields the critical points and the corresponding critical forcing

$$x_c = \pm\frac{x_0}{\sqrt{3}} \qquad \theta_c = \mp\frac{2}{3\sqrt{3}}. \tag{10}$$

We will consider cases in which x is initiated at the negative fixed point. For $\theta = 0$ this is $x(t = 0) = -x_0 = -1$. There are three equilibrium solutions, two stable and one unstable one. In the potential landscape, this translates to two minima and a saddle. With increasing forcing, the left minimum starts to rise and become flatter. When the internal time scale of system allows it to react to the change quickly enough, this leads to critical slowing down. At the critical forcing, the minimum ceases to exist and the state starts moving to the other equilibrium. Due to inertia, this happens in a finite transition time.

Scaling law for transition time

The derivation of the time delay between the tipping point and the tipping temperature is based on the concept of the delayed bifurcation of non-autonomous systems [30, 33, 34]. In the main text, we extend this to the delay between tipping temperature and point of no return. Since we are interested in the time scaling of the trajectory close to the fold, we expand around the critical point and forcing (x_c, θ_c), where $\delta x = x - x_c$ and obtain

$$\dot{\delta x} = \frac{x_0}{2\tau_s}\left[-\frac{3x_c}{x_0^3}(\delta x)^2 + (\theta - \theta_c)\right] \tag{11}$$

Absorbing all dimensional system parameters into the two scales X_{scale} and T_{scale} and introducing the dimensionless variables $\tilde{x} = \delta x / X_{scale}$ and $\tilde{t} = (t - t_c)/T_{scale}$ yields

the universal normal form

$$\frac{d\tilde{x}}{d\tilde{t}} = -\tilde{x}^2 + \tilde{t} \tag{12}$$

with

$$T_{scale} \sim \tau_f^{1/3}\tau_s^{2/3}, \qquad X_{scale} \sim \tau_f^{-1/3}\tau^{1/3}. \tag{13}$$

Close to the critical point, all saddle node bifurcations reduce to the same dynamics, described by the universal normal form. The rescaling parameters then tell us how the internal time scale of the system and the forcing time scale shape the transition. For all saddle node bifurcations, the length of the transition time scales with T_{scale} and the associated state differences scale with X_{scale}. The full derivation can be found in the Supplementary Note 2.

Tipping phases

The three dynamical points tipping temperature, tipping point and point of no return define five qualitatively different phases of tipping. The three points are marked in Fig. 1a as dashed lines and the phases as the shading in the background.

The gradual phase In the gradual phase (blue phase in Fig.1), the state of the system only weakly responds to the forcing. The system tracks the slowly changing equilibrium and as such is in quasi-equilibrium. Variance might slowly start to increase as the system moves closer towards the tipping temperature but does not yet reach values that are significantly higher than its equilibrium value.

The tipping approach The closer the system moves towards the tipping temperature, the more it starts to lose its restoring abilities. Small deviations now have a larger impact, because the system can not immediately heal itself and restore the equilibrium value. This is the phase in which critical slowing down (CSD) becomes prominent and the unpredictability caused by larger fluctuations in the system starts to rise. The variance increase of the system starts to accelerate. The tipping approach phase terminates with the reaching of the tipping temperature (yellow phase in Fig. 1a). Note that the gradual phase and the tipping approach might not be clearly distinguishable for systems in which the internal time scale τ_s is very large compared to the forcing time scale and the quasi-equilibrium condition is not given to begin with.

The inertia phase The inertia phase is the phase after the crossing of the tipping temperature, but before the system state has reached the tipping point (orange phase in Fig. 1a). As discussed above, due to the inertia of the system there is a finite transition time between the crossing of the critical forcing and the systems reaction (Fig. 3). While the system still lingers close to the ghost of the old equilibrium, it has nothing to restore to anymore. In this sense, the system is in a state of free fall, in which perturbations can not be damped anymore and the system is highly unstable. The

fluctuation variance within the system increases to its maximum value, increasing the unpredictability of the system. In our simulations, the variance increases up to 300%.

The escape phase Once the tipping point has been crossed, the true acceleration towards the new equilibrium begins. The trajectory starts changing very quickly and the self amplifying feedback dominates the dynamics (red phase in Fig. 1a). The trajectory escapes the region located close to the ghost of the old equilibrium. In this phase, fluctuations start being suppressed by the strong drift. The system gets dragged towards the new equilibrium so quickly that it does not have time to amplify or dampen fluctuations anymore, but is dominated by the deterministic drift. Reversibility of the tipping is still given, if the forcing is reduced to its initial value almost instantaneously. In this regime, the unpredictability caused by fluctuations starts decreasing, but is still high (100%-200% increase in Fig. 1).

The convergence phase After the point of no return has been crossed, even a complete, immediate elimination of the forcing can not keep the system from converging to the new equilibrium anymore. The system keeps moving towards the new basin of attraction (Fig. 1c) with increasing velocity (green phase in Fig. 1a). Fluctuations continue being repressed. The convergence phase ends once the system has reached the new equilibrium, after which it settles. The fluctuation variance also settles to its new equilibrium value.

Variance equation

To derive an expression for the variance along the whole trajectory, Eq. (6) is expanded around the deterministic solution up to linear order $\delta x = x - x_{det}$. Here, variance includes the fluctuations around the mean state and the deviation between possible trajectory evolutions. For white noise, one can directly average the evolution of δx^2 over noise realisations which yields a linearised equation for $V = \langle \delta x^2 \rangle$

$$\frac{dV}{dt} = \frac{1}{\tau_s}\left(1 - 3\left(\frac{x_{det}}{x_0}\right)^2\right)V + g. \tag{14}$$

where g is the noise intensity for white noise. For red noise, the derivation involves expanding and solving the two dimensional system of equations Eqs. (6), (7). Under some quasi equilibrium assumptions (see Supplementary Note 3) and for noise time scales much smaller than the system time scale the equation reduces to the same simple form

$$\frac{dV}{dt} = 2\lambda(t)V(t) + 2\sigma^2\tau_n \tag{15}$$

where the noise time scale now only enters the constant noise injection term. The solution of the variance equation is

$$V(t) = V(t_0)e^{\int_{t_0}^{t} 2\lambda(u)du} + 2\sigma^2\tau_n \int_{t_0}^{t} e^{\int_{t}^{s} 2\lambda(u)du} ds. \tag{16}$$

For a comprehensive derivation see Supplementary Note 3. The first term in the variance equation describes how fluctuations grow or decay locally, depending on the sign of the restoring force $\partial_x f(x_{det})$. The second term is a constant noise contribution. Since the variance here describes how much trajectories deviate from the deterministic trajectory, we can think of this equation as a description of the spread of possible trajectories. Before the tipping point, all trajectories are still located relatively close to the deterministic trajectory, so the equation describes the increase of the fluctuations around the mean state. This is what the critical slowing down (CSD) framework usually tries to capture, where the weakening of the restoring force is used to indicate the approach of the tipping temperature. In that sense, before the tipping point, the variance equation still mainly describes the fluctuation variance.

The closer we get to the tipping point, and especially during the tipping, the trajectories start to deviate strongly from each other. Since the equation does not separate between fluctuations around the mean state of a single trajectory and the spread of trajectories within the ensemble, the latter dominates in this regime, so unpredictability mainly stems from the large spread of possible trajectories. One should thus think of the variance equation as describing the uncertainty at a specific time and state of the system along the tipping process.

The stability of the system can also be understood in terms of the local growth rate $\lambda(t) = \frac{1}{\tau_s}(1 - 3(x_{det}/x_0)^2)$. In the variance equation, the growth rate indicates how much variance is damped or amplified by the stability of the system. For $x_{det} < -|x_c|$, so before the tipping point is reached λ acts as a restoring rate that tries to bring the state back to its equilibrium after a perturbation. The closer the system gets to the tipping point, the smaller the restoring abilities become, until $\lambda = 0$ at $x_{det} = -|x_c|$. For $-|x_c| < x_{det} < |x_c|$, the local growth rate becomes a positive amplification rate, with the maximal value reached at the point of no return $x = 0$. In this regime the trajectories start to escape at slightly different times, which leads to a large spread in system states at the same time t (cf. Fig. S1). Plotted over the system state x instead of time, this means that the spread in possible future evolutions of the system based on the current system state becomes much larger (cf. Fig. S1), greatly increasing its unpredictability. For $x_{det} > |x_c|$, the local growth rate becomes negative again and the system is now restored to its new equilibrium state.

Data availability

The data underlying all figures are available at Zenodo (https://doi.org/10.5281/zenodo.23166586). The full simulation ensembles are not archived because of their size, but can be regenerated with the code provided (see Code availability) using the fixed random seeds.

Code availability

The code used to generate the simulation ensembles and figures is available at Zenodo (https://doi.org/10.5281/zenodo.23166586).

Supplementary information

Supplementary information, containing the comprehensive derivations of all equations in the main text, is available in the accompanying file.

Acknowledgements

The authors gratefully acknowledge the Ministry of Research, Science and Culture (MWFK) of Land Brandenburg for supporting this project by providing resources on the high performance computer system at the Potsdam Institute for Climate Impact Research.

Funding

This paper is supported by the EconX project of the Max Planck Institute of Geoanthropology in Jena. The EconX project (2023 FWF 0002) is funded by the "FTI-Thüringen-Forschung" programme as part of the umbrella brand "Thüringen MOTIVation". The research was financially supported by the Studienstiftung des deutschen Volkes e.V. foundation, who did not have any influence on the study design, the data analysis, or the interpretation of the results (nor any other influence).

Author contributions

A. Levermann conceived the study. N. Doerfler and A. Levermann developed the conceptual framework. N. Doerfler performed all simulations and led the analysis, with contributions from A. Levermann. N. Doerfler wrote the manuscript with input from A. Levermann.

Competing interest

The authors declare no competing interests.

References

[1] Lenton, T. M. *et al.* Tipping elements in the earth's climate system. *Proceedings of the National Academy of Sciences* **105**, 1786–1793 (2008).

[2] Armstrong McKay, D. I. *et al.* Exceeding 1.5°c global warming could trigger multiple climate tipping points. *Science* **377**, eabn7950 (2022).

[3] Rignot, E., Mouginot, J., Morlighem, M., Seroussi, H. & Scheuchl, B. Widespread, rapid grounding line retreat of pine island, thwaites, smith, and kohler glaciers, west antarctica, from 1992 to 2011. *Geophysical Research Letters* **41**, 3502–3509 (2014). URL https://agupubs.onlinelibrary.wiley.com/doi/abs/10.1002/2014GL060140.

[4] Joughin, I., Smith, B. E. & Medley, B. Marine ice sheet collapse potentially under way for the thwaites glacier basin, west antarctica. *Science* **344**, 735–738 (2014). URL https://www.science.org/doi/abs/10.1126/science.1249055.

[5] Robinson, A., Calov, R. & Ganopolski, A. Multistability and critical thresholds of the greenland ice sheet. *Nature Climate Change* **2**, 429–432 (2012). URL https://doi.org/10.1038/nclimate1449.

[6] Boulton, C. A., Lenton, T. M. & Boers, N. Pronounced loss of amazon rainforest resilience since the early 2000s. *Nature Climate Change* **12**, 271–278 (2022).

[7] Stommel, H. Thermohaline convection with two stable regimes of flow. *Tellus* **13**, 224–230 (1961).

[8] Rahmstorf, S. On the freshwater forcing and transport of the atlantic thermohaline circulation. *Climate Dynamics* **12**, 799–811 (1996).

[9] Zemp, D. C. *et al.* Self-amplified amazon forest loss due to vegetation-atmosphere feedbacks. *Nature communications* **8**, 14681 (2017).

[10] Garbe, J., Albrecht, T., Levermann, A., Donges, J. F. & Winkelmann, R. The hysteresis of the antarctic ice sheet. *Nature* **585**, 538–544 (2020).

[11] Lenton, T. M. Early warning of climate tipping points. *Nature Climate Change* **1**, 201–209 (2011).

[12] Boers, N., Marwan, N., Barbosa, H. M. & Kurths, J. A deforestation-induced tipping point for the south american monsoon system. *Scientific reports* **7**, 41489 (2017).

[13] Lovejoy, T. E. & Nobre, C. Amazon tipping point (2018).

[14] Dakos, V. *et al.* Tipping point detection and early warnings in climate, ecological, and human systems. *Earth System Dynamics* **15**, 1117–1135 (2024).

[15] Boers, N. Observation-based early-warning signals for a collapse of the atlantic meridional overturning circulation. *Nature Climate Change* **11**, 680–688 (2021).

[16] Smith, T., Morr, A., Bookhagen, B. & Boers, N. Predicting instabilities in transient landforms and interconnected ecosystems. *Nature Communications* **17**, 1316 (2026).

[17] Hirota, M., Holmgren, M., Van Nes, E. H. & Scheffer, M. Global resilience of tropical forest and savanna to critical transitions. *Science* **334**, 232–235 (2011).

[18] Jackson, L. C. *et al.* Global and european climate impacts of a slowdown of the amoc in a high resolution gcm. *Climate dynamics* **45**, 3299–3316 (2015).

[19] Aschwanden, A. *et al.* Contribution of the greenland ice sheet to sea level over the next millennium. *Science advances* **5**, eaav9396 (2019).

[20] Wunderling, N. *et al.* Climate tipping point interactions and cascades: a review. *Earth System Dynamics* **15**, 41–74 (2024).

[21] Rocha, J. C., Peterson, G., Bodin, Ö. & Levin, S. Cascading regime shifts within and across scales. *Science* **362**, 1379–1383 (2018).

[22] Liu, T. *et al.* Teleconnections among tipping elements in the earth system. *Nature Climate Change* **13**, 67–74 (2023).

[23] Nordhaus, W. Economics of the disintegration of the greenland ice sheet. *Proceedings of the National Academy of Sciences* **116**, 12261–12269 (2019).

[24] Kopp, R. E., Shwom, R. L., Wagner, G. & Yuan, J. Tipping elements and climate–economic shocks: Pathways toward integrated assessment. *Earth's Future* **4**, 346–372 (2016).

[25] Dietz, S., Rising, J., Stoerk, T. & Wagner, G. Economic impacts of tipping points in the climate system. *Proceedings of the National Academy of Sciences* **118**, e2103081118 (2021).

[26] Levermann, A. 'climate free fall': why the biggest risk to our economies is yet to be recognized. *Nature* **655**, 571–573 (2026). URL http://dx.doi.org/10.1038/d41586-026-02154-8.

[27] Dakos, V. *et al.* Slowing down as an early warning signal for abrupt climate change. *Proceedings of the National Academy of Sciences* **105**, 14308–14312 (2008).

[28] Van Passel, J. *et al.* Critical slowing down of the amazon forest after increased drought occurrence. *Proceedings of the National Academy of Sciences* **121**, e2316924121 (2024).

[29] Kuehn, C. A mathematical framework for critical transitions: Bifurcations, fast–slow systems and stochastic dynamics. *Physica D: Nonlinear Phenomena* **240**, 1020–1035 (2011).

[30] Berglund, N. & Gentz, B. Metastability in simple climate models: pathwise analysis of slowly driven langevin equations. *Stochastics and Dynamics* **2**, 327–356 (2002).

[31] Clarke, J., Huntingford, C., Ritchie, P. D. & Cox, P. Conditions for skilful spatial and temporal tipping point early warning signals. *Journal of Physics: Complexity* **7**, 025007 (2026).

[32] Levermann, A. *et al.* Potential climatic transitions with profound impact on europe: Review of the current state of six 'tipping elements of the climate system'. *Climatic Change* **110**, 845–878 (2012).

[33] Li, J. H., Ye, F. X.-F., Qian, H. & Huang, S. Time-dependent saddle–node bifurcation: Breaking time and the point of no return in a non-autonomous model of critical transitions. *Physica D: Nonlinear Phenomena* **395**, 7–14 (2019).

[34] Haberman, R. Slowly varying jump and transition phenomena associated with algebraic bifurcation problems. *SIAM Journal on Applied Mathematics* **37**, 69–106 (1979).

[35] Berglund, N. & Kunz, H. Memory effects and scaling laws in slowly driven systems. *Journal of Physics A: Mathematical and General* **32**, 15–39 (1999).

[36] Boulton, C. A., Lenton, T. M. & Boers, N. Pronounced loss of amazon rainforest resilience since the early 2000s. *Nature Climate Change* **12**, 271–278 (2022).

[37] Flores, B. M. *et al.* Critical transitions in the amazon forest system. *Nature* **626**, 555–564 (2024).

[38] Ditlevsen, P. & Ditlevsen, S. Warning of a forthcoming collapse of the atlantic meridional overturning circulation. *Nature Communications* **14**, 4254 (2023). URL https://doi.org/10.1038/s41467-023-39810-w.

[39] Mehling, O., Börner, R. & Lucarini, V. Limits to predictability of the asymptotic state of the atlantic meridional overturning circulation in a conceptual climate model. *Physica D: Nonlinear Phenomena* **459**, 134043 (2024).

[40] Ritchie, P. D., Clarke, J. J., Cox, P. M. & Huntingford, C. Overshooting tipping point thresholds in a changing climate. *Nature* **592**, 517–523 (2021).

[41] Ritchie, P., Karabacak, Ö. & Sieber, J. Inverse-square law between time and amplitude for crossing tipping thresholds. *Proceedings. Mathematical, Physical, and Engineering Sciences* **475**, 20180504 (2019).

[42] van der Bolt, B., van Nes, E. H. & Scheffer, M. No warning for slow transitions. *Journal of the Royal Society Interface* **18**, 20200935 (2021).

[43] Ben-Yami, M., Morr, A., Bathiany, S. & Boers, N. Uncertainties too large to predict tipping times of major earth system components from historical data. *Science Advances* **10**, eadl4841 (2024).

[44] Ashwin, P., Wieczorek, S., Vitolo, R. & Cox, P. Tipping points in open systems: bifurcation, noise-induced and rate-dependent examples in the climate system. *Philosophical Transactions: Mathematical, Physical and Engineering Sciences* 1166–1184 (2012).

[45] Ritchie, P. & Sieber, J. Early-warning indicators for rate-induced tipping. *Chaos: An Interdisciplinary Journal of Nonlinear Science* **26** (2016).

[46] Wieczorek, S., Xie, C. & Ashwin, P. Rate-induced tipping: Thresholds, edge states and connecting orbits. *Nonlinearity* **36**, 3238–3293 (2023).

[47] Lohmann, J. & Ditlevsen, P. D. Risk of tipping the overturning circulation due to increasing rates of ice melt. *Proceedings of the National Academy of Sciences* **118**, e2017989118 (2021).

[48] Börner, R., Mehling, O., Von Hardenberg, J. & Lucarini, V. Global stability of the atlantic overturning circulation: Edge state, long transients and boundary crisis under co _2 forcing. *arXiv preprint arXiv:2504.20002* (2025).

[49] Kypke, K. *et al.* Chaotic fluctuations in greenland ice streams limit predictability of ice sheet collapse. *Earth System Dynamics* **17**, 769–794 (2026).

Supplementary Files

This is a list of supplementary files associated with this preprint. Click to download.

- doerflerlevermann26bsupp.pdf